Asgard ESCRT-IIIs assemble into helical filaments in the presence of DNA and remodel eukaryotic membranes

Nataly Melnikov[1,2], Dikla Nachmias[1,2], Gal Halbi[3], Alexander Upcher[4], Ran Zalk[4], Ann Bernheim-Groswasser[3,4], Natalie Elia[1,2]

1 Department of Life Sciences, Ben-Gurion University of the Negev, Beer Sheva 84105, Israel

2 National Institute for Biotechnology in the Negev (NIBN), Ben-Gurion University of the Negev, Beer Sheva 84105, Israel

3 Department of Chemical Engineering, Ben-Gurion University of the Negev, Beer Sheva 84105, Israel

4 Ilse Katz Institute for Nanoscale Science and Technology, Ben Gurion University of the Negev, Beer Sheva 84105, Israel

* Corresponding author:
Natalie Elia
Phone: 972-8-6428735
Email: elianat@post.bgu.ac.il

ABSTRACT

The ESCRT machinery mediate membrane remodeling in numerous processes in cells including cell division and nuclear membrane reformation. The identification of ESCRT homologs in Asgard archaea, currently considered the closest ancestor of eukaryotes, suggests a role for ESCRTs in the membrane remodeling processes that occurred during eukaryogenesis. Yet, the function of these distant ESCRT homologs is mostly unresolved. Here we show that Asgard ESCRT-III proteins self-assemble into homo- and hetero- helical tubes, a hallmark of the eukaryotic ESCRT system. Asgard ESCRT-III tube assembly was facilitated in the presence of DNA and inhibited by DNAase. Notably, Asgard ESCRT-III filaments remodeled eukaryotic-like membrane vesicles, also in the presence of DNA, indicating an ancient role for the ESCRT complex in membrane remodeling, that may involve DNA binding. The ability of Asgard archaeal ESCRTs to remodel eukaryotic-like membranes, places them at the junction between prokaryotes and eukaryotes, substantiating a role for ESCRTs in eukaryogenesis.

INTRODUCTION

The Asgard superphyla, manifest a unique branch that, according to current evolutionary theories, is considered to be the closest prokaryotic relative of eukaryotes. All Asgard archaeal species were found to encode for Eukaryotic Signature Proteins (ESPs), that carry cellular functions that until recently were considered as exclusive to eukaryotes (1-3). Thus, Asgard proteins potentially hold the core functions of ancient eukaryotic cellular machines. Of particular interest, are ESPs with membrane remodelling capabilities, as these proteins may contribute to the establishment of cellular compartmentalization during eukaryogenesis. Indeed, Asgard archaea encode for several eukaryotic membrane remodelling machineries including the SNARE complex, BAR domains proteins and the ESCRT machinery (1, 3, 4). Among these machineries, ESCRTs are the most conserved and are encoded by all Asgard species

62 discovered up to date, suggesting that they carry essential functions in these unique
63 prokaryotes (5, 6).
64
65 The ESCRT machinery constitute one of the most robust and versatile cellular
66 apparatus for membrane constriction and fission. Proteins of the machinery are
67 encoded by all domains of life and were shown to mediate membrane remodelling in a
68 wide range of eukaryotic cellular membranes including plasma membrane, nuclear
69 membrane and endocytic membranes (7, 8). Moreover, ESCRT-mediated processes
70 span a large spectrum of length scales, from less than 100 nm for vesicle release to up
71 to 1 μm for cell division. How the ESCRT complex mediate membrane remodelling in
72 this large landscape of membrane sources and length scales is mostly unknown (9).
73
74 The eukaryotic ESCRT system is composed of five subfamilies, i.e. ESCRT 0-III and the
75 AAA-ATPase VPS4. Within this complex, ESCRT-III (named CHMPs in animal cells)
76 and VPS4 manifest the minimal unit required for driving membrane fission (9, 10).
77 According to current models, membrane constriction and scission are mediated by
78 polymerization of ESCRT-III proteins into helical hetero-filaments and their remodelling
79 by VPS4 (10-14). Indeed, ESCRT-III proteins have been shown organize in helical
80 filaments and tubes both in vitro and in cells (14-19). However, the large number of
81 proteins within the ESCRT-III subfamily —twelve in humans and eight in yeast - have
82 challenged mechanistic studies of the basic function of the machine.
83
84 Reduced, simplified ESCRT-III systems have been identified in prokaryotes including in
85 bacteria and archaea (named Vipp1 and PspA in bacteria and CdvB in archaea) (7, 20,
86 21). While the bacterial homologs were shown to remodel membranes in vitro, no VPS4
87 was identified in this system so far, and whether these distant homologs can sever
88 membranes has not been clarified. ESCRTs encoded by TACK archaea were shown to
89 participate in cell division, suggesting functional similarities between the eukaryotic and
90 archaeal ESCRT systems (22-25). Within the archaeal domain the Asgard ESCRT
91 system is considerably closer to the eukaryotic system. While all other archaea encode
92 only for homologs of the ESCRT-III/VPS4 module, Asgard archaea encode for

homologs of the complete ESCRT system (ESCRT-I-III and VPS4) (6, 7). Additionally, the sequence of Asgard ESCRT-III/VPS4 proteins is more closely related to those of eukaryotes than to other archaeal ESCRT systems (the CDV system) (5, 20). Lastly, VPS4 homologs of Asgard archaea were shown to functionally interact with eukaryotic ESCRTs in both yeast and mammalian cells (5, 26). Notably, the Asgard ESCRT-III subfamily is substantially reduced compared to eukaryotes with only two ESCRT-III proteins (named here CHMP1-3 and CHMP4-7) encoded in some species including Loki and Heimdall archaeota (1, 5, 7, 26). Hence, the Asgard ESCRT system constitutes a minimalist ESCRT machinery that may hold the core capabilities of eukaryotic ESCRTs and could have been involved in membrane remodelling processes that occurred during eukaryogenesis. Yet, the function, organization, and properties of Asgard ESCRT-III complexes as well as their ability to remodel membranes are mostly unknown.

In this work, we provide the first evidence that Asgard ESCRT-III complexes share functional similarities with eukaryotic ESCRTs. Using purified ESCRT-III homologs encoded by the most abundant Asgard phyla, Lokiarchaeota (Loki), we show that the Asgard ESCRT-III protein CHMP4-7 self-assemble into homo- and hetero- helical tubes that resemble those of eukaryotes (15, 18, 19, 27). The proportion of helical tubes was dramatically enriched in the presence of short DNA oligos, while no filaments could be observed upon DNAse treatment. Notably, Loki ESCRT filaments, formed under any of these conditions, were able to bind and deform small unilamellar vesicles (SUVs) comprised of eukaryotic-like synthetic phospholipids. Hence, Loki ESCRT-III assemble into helical filaments that are affected by oligonucleotides and are capable of remodelling eukaryotic-like membranes.

RESULTS

Eukaryotic ESCRT-III proteins polymerize into helical filaments - a hallmark of ESCRT-III organization that is thought to be essential for their function in membrane remodeling

124 (8, 28). Polymerization is mediated by the snf7 domain that is conserved in both
125 archaea and eukaryotes, but the polymerization properties of Asgard ESCRT-III has not
126 been examined (5, 20, 26). To investigate the assembly properties of Asgard ESCRT-III
127 proteins, we purified recombinant versions of the ESCRT-III proteins CHMP4-7 and
128 CHMP 1-3, encoded by the Loki GC14_75 strain (KKK44605.1 and KKK42122.1,
129 respectively). Using our assay conditions (see material and methods), full length CHMP
130 4-7 self-assembled into filaments (Fig 1). No filaments were observed under the same
131 conditions using full length CHMP1-3 (sup Fig. 1A). In negative stain TEM images,
132 CHMP 4-7 was predominantly seen in either long, thin filaments or rod-shaped tubes
133 (Fig 1A, see arrows). A pattern of parallel, periodic stripes was detected in the CHMP 4-
134 7 tube structures by cryo-EM, supporting a helical tube organization (Fig 1B, C). The
135 outer diameter of the CHMP4-7 tubes was variable, ranging between 35 to 55 nm
136 (averaged diameter 44nm ± 30.9). Tube length was typically between 300 - 450 nm (Fig
137 1D). The overall shape of CHMP4-7 helical tubes resembled the helical tubes previously
138 described for eukaryotic or bacterial ESCRT-III filaments (15, 18, 19, 29). The diameter
139 of Loki CHMP 4-7 helical tubes was slightly larger than the diameters measured for
140 human CHMP1B (~25nm) or the bacterial ESCRT III homologs PspA (~21 nm), but was
141 in the range of diameters measured for human CHMP2A-CHMP3 (38-43 nm) (18, 19,
142 29). Collectively, these data indicate that Loki CHMP 4-7 spontaneously self-assemble
143 into the typical helical tube organization described for the ESCRT-III complex.
144
145 Next, we examined whether, similar to their human homologs, Loki ESCRT-IIIs can
146 assemble into co-polymers (18, 19). To this end, full lengths Loki CHMP4-7 and CHMP
147 1-3 were incubated at different ratios. While no filaments were seen at 1:1 CHMP4-7-
148 CHMP1-3 ratio, helical tubes could be readily observed at 2:1, 4:1 and 6:1 ratios (Fig 2
149 and Sup Fig 1B). Notably, CHMP 4-7-CHMP 1-3 helical tubes exhibited different
150 properties than those observed for the CHMP 4-7 homo-polymer. First, their outer
151 diameter was significantly smaller and less diverse (CHMP 4-7-CHMP 1-3 2:1 ratio,
152 31±7.7) (Fig. 2B, left panel). Second, helical tubes formed in the presence of both
153 CHMP4-7 and CHMP1-3 were significantly longer than those formed by the CHMP4-7
154 homo-polymer (>X1.5 folds increase for 2:1 and 4:1 ratios) (Fig. 2B, right panel). Third,

155 the morphology of the CHMP4-7-CHMP1-3 helical tube was slightly different: tubes
156 appeared to be more curved and the periodic stripes, which could only be observed by
157 cryo-EM for CHMP 4-7 homo-polymers, were readily detected in negative stain images
158 of the co-polymer, suggesting that packing of the helical tube is less tight in the
159 presence of CHMP1-3 (Fig 2A). These phenotypic changes were not induced upon
160 substituting CHMP 1-3 with purified GFP, suggesting that they are specifically
161 contributed by CHMP 1-3 (Sup. Fig 1C). We therefore concluded that Loki ESCRT-III
162 proteins assemble into helical tubes composed of homo- and co-polymers with the co-
163 polymers forming longer, narrower, and more homogenous tubes than the homo-
164 polymer. These findings are in line with previous observations obtained for human
165 ESCRT-III CHMP1B homo- and co-polymers (in the presence of IST1), which also
166 formed a narrower, more uniform tubes in the co-polymer composition (30). The
167 realization that both human and Asgard ESCRT-III proteins assemble into homo-and
168 co- polymers with the latter adopting a narrower more uniform tube shape, strongly
169 suggests that this is a basic, conserved property of the ESCRT-III system.
170
171 Recent work from our laboratory showed that purified Loki CHMP4-7 binds short DNA
172 oligonucleotides (26). Human CHMP1B, exhibited similar properties and a recently
173 solved cryo-EM structure of human CHMP1B/IST1 filaments demonstrated direct
174 interactions between the ESCRT-III filament and nucleic acids (26, 31). We, therefore,
175 set to examine the effect of short DNA oligonucleotides on the self-assembly properties
176 of Asgard ESCRT-III filaments. A significant increase in helical tube assemblies was
177 observed for the co-polymer in the presence of ssDNA, in both negative stain- and cryo-
178 TEM images (Fig 3A-B and Sup Fig 2A). More helical tubes were also observed upon
179 addition of dsDNA, but to a lower extent. No filaments were observed when incubating
180 CHMP1-3 with DNA, indicating that that observed increase in helical tubes do not result
181 from self-assembly of CHMP1-3 into homo-polymers (Sup Fig. 2D). Addition of ssDNA
182 to CHMP4-7 homo-polymers also led to a dramatic increase in helical tubes, indicating
183 that the effect of DNA is not restricted to the co-polymer (Fig. 3C, Sup Fig 2B). The
184 presence of DNA also affected the properties of the helical tubes. CHMP 4-7-CHMP1-3
185 helical tubes formed in the presence of either ds- or ss- DNA exhibited larger and more

186 variable diameters (43.9nm ±58 for CHMP4-7-CHMP1-3 2:1 ssDNA vs CHMP4-7-
187 CHMP1-3 2:1 31nm ±7.7), resembling the diameter measured for the CHMP 4-7 homo-
188 polymer (CHMP4-7 44nm ±30.9) (Fig. 3D). Moreover, filaments were less curved, and
189 the periodic stripes observed in negative stain images in the co-polymer could not be
190 observed (Fig 3A). Addition of DNA did not affect the characteristics length or diameter
191 of tubes formed by CHMP 4-7 homo-polymers (Fig. 3D-E). It, therefore, appears that
192 DNA aids the organization of Loki-ESCRT-III proteins into helical tubes and counteract,
193 at least to some extent, the effect of CHMP1-3 on tube characteristics.
194
195 To further investigate the possible effect of DNA on Loki ESCRT-III polymerization, we
196 performed the self-assembly reaction in the presence of DNase. Surprisingly, filament
197 formation was completely abolished for both homo- and co-polymers in the presence of
198 DNase (Fig 3F and Sup Fig. 2E-F). Additionally, no filaments were observed upon
199 incubation with DNAse post self-assembly, suggesting that filament stability and/or
200 integrity are dependent on DNA. Altogether, these findings strongly suggest that DNA is
201 an essential component of Loki ESCRT-III filamentous organization.
202
203 Eukaryotic ESCRT-IIIs were shown to bind and deform membranes *in vitro* and in cells
204 (28). To determine whether ESCRTs encoded by Asgard archaea carry the ability to
205 remodel membranes, we incubated Loki ESCRT-III pre-assembled filaments with small
206 unilamellar vesicles (SUVs, ~100 nm) composed of negatively charged eukaryotic-like
207 phospholipids (1:1, PC:PS). Under these conditions, ESCRT-III filaments, assembled
208 under any of the conditions described above (including in the presence of DNA), were
209 found to intimately interact with SUVs (Fig. 4A, B and Sup Fig. 3). We identified four
210 main types of ESCRT-III-SUV interactions: (1) Attachment of the SUV to the outside
211 surface of the tube, which was associated with flattening of the vesicle at the filament-
212 vesicle interface; (2) Docking of the SUV at the tip of the helical tube; (3) Invagination of
213 the SUV to the interior of the ESCRT-III tube; and (4) Dramatic remodeling of both the
214 SUV and the ESCRT-III tube (see examples in Fig. 4C, left panel). Combinations of
215 several types of interactions on the same filament were also observed, indicating that
216 these interactions are not mutually exclusive. Moreover, a docked SUV that invaginates

217 the helical tube was observed occasionally (Fig. 4B, left panel and sup movies 1, 2),
218 suggesting that these two types of interactions represent successive steps.
219 Invaginations of more than one vesicle to the same tube could be observed, in cryo-
220 TEM and cryo-tomography reconstructions, giving rise to the formation of a complex
221 membrane system with several vesicles internalized into one another (Fig 4B, and sup
222 movies 1, 2). In these complex organizations, which were often accompanied by a
223 considerable deformation of both the filament and the vesicles, the characteristics
224 periodic stripes of the ESCRT-III filament could often be detected at the exterior of the
225 filament-vesicle complex, suggesting that the observed morphologies result from
226 internalization of vesicles into the ESCRT-III helical tube followed by deformation of the
227 tube. Loki ESCRT III filaments also interacted with neutrally charged SUVs (100% PC)
228 but to a much lower extent, exhibiting predominantly binding of the SUV on the outside
229 of the helical tube (Sup Fig. 4). Therefore, Loki ESCRT-III filaments associate with
230 eukaryotic-like membrane vesicles, and deform negatively charged vesicles via the
231 interior of the tube (see proposed model in Fig. 4D).
232
233 Last, we asked whether the composition of ESCRT-III helical tubes, described here,
234 affect their capabilities to remodel membranes. Because vesicle-filaments interactions
235 were identified under all conditions, we analyzed the proportion of the four types of
236 filament-vesicle interaction, we identified, in different ESCRT-III compositions. No
237 difference was observed in the distributions of homo- and co- polymers, suggesting that
238 the composition of the filament does not significantly affect membrane indications. The
239 presence of DNA affected the distributions of ESCRT-III-SUV interactions in both the
240 homo- and co- polymers, as follows (Fig. 4C): (1) The association of vesicles with the
241 outside surface of the helical tube was considerably enriched (outside, type 1, No DNA,
242 <15%; with DNA, >35%). (2) Interactions with the tip of the filament (docking, type 2)
243 and invagination of the vesicle (inside, type 3) were significantly enriched. (3) The
244 extent of complete remodeling events (remodeling, type 4) was dramatically reduced
245 (with DNA, ~5%; no DNA ~80%). Therefore, homo- and co- Loki ESCRT-III filaments
246 are capable of interacting and remodeling lipid membranes, both in the presence and

247 absence of DNA, but the extent of remodeling appear to be attenuated by the presence
248 of DNA.
249
250 DISCUSSION
251
252 In this work, we provide the first evidence to show that, similar to their eukaryotic
253 homologs, Asgard ESCRT-III proteins assemble into helical filaments that remodel
254 membranes. These findings confirm that ESCRT homologs encoded by Asgard archaea
255 are functionally related to their eukaryotic homologs. We further provide data to support
256 prominent role for DNA in the Asgard ESCRT-III system. Finally, by using SUVs
257 composed of eukaryotic phospholipids, which are fundamentally different from archaeal
258 lipids, we demonstrate that the Asgard ESCRT-III could, in-principle, contribute to the
259 membrane remodeling processes that occurred during eukaryogenesis and gave rise to
260 the complex phospholipids-based endomembrane system of eukaryotes.
261
262 Our data point to similarities between the human and Asgard ESCRT-III systems. First,
263 the nature of self-assembly appear to be conserved. Similar to the human CHMP1B-
264 IST1 complex, Loki CHMP4-7 was found to polymerize alone or in the presence of
265 CHMP 1-3, with the homo-polymer exhibiting a wider, more variable diameter compared
266 to the co-polymer (30). What controls the diameter of the ESCRT-III helical tube is
267 currently unknown. Our findings that, similar to their human homologs, Asgard ESCRT-
268 III homo-filaments can adopt a wide range of diameters that can be tuned by the
269 addition of another ESCRT-III components, strongly suggest that this is a conserved
270 feature of the ESCRT-III system. Therefore, a basic feature of the ESCRT-III system
271 may be their ability to assemble into flexible homo filaments that can be tuned to adopt
272 different shapes by incorporating additional ESCRT-III proteins into the polymer. Such a
273 model can explain how the ESCRT-III system execute the large repertoire of membrane
274 remodeling processes in cells, which greatly vary in scales and topologies (7, 8).
275 The topology of membrane binding, described here for Loki ESCRT-IIIs, resemble the
276 topology reported for the human CHMP1B-IST1 polymer, i.e. bindings via the interior of
277 the helical tube (30). This topology is reversed to the conventional topology attributed to

278 the ESCRT complex and that was described for the CHMP2A-CHMP3 co-polymer (19,
279 27), which is binding and deforming membranes via the external surface of the tube.
280 Reversed membrane binding topology was also recently reported for the bacterial
281 ESCRT-III homologs Vipp1 and PspA (29, 32). Whether this topology represent the
282 preferred topology of ancient ESCRTs or is a consequence of the experimental, in vitro,
283 system is yet to be determined. Regardless, these similarities suggest that the ESCRT-
284 III membrane remodeling properties reported here are a common property of the
285 ESCRT system, conserved in all domains of life.
286
287 Our results highlight DNA as an essential Loki ESCRT-III partner. Organization of both
288 homo- and co- ESCRT-III polymers into helical tubes was enhanced in the presence of
289 short DNA oligonucleotides and helical tube formation was completely blocked upon
290 addition of DNase. Whether DNA has a role in stabilizing Loki ESCRT-III filaments or in
291 facilitating their nucleation is still unknown. Notably, human CHMP1B-IST1 filaments
292 were shown to bind DNA in the inner side of the tube (31). Additionally, nucleotides
293 were recently resolved in cryo-EM structures of the bacterial ESCRT-III Vipp1 and were
294 suggested to play a role in helical tube stabilization (32). It is therefore tempting to
295 speculate that nucleotide binding is an additional core property of the ESCRT-III
296 machine that is conserved in all domains of life.
297
298 Our data show that Loki ESCRT-III filaments that polymerized in the presence of DNA
299 were able to bind and deform membrane vesicles. Yet, the extent of membrane
300 deformation that occurred inside the tube was attenuated, while binding on the exterior
301 of the ESCRT-III tube was enhanced. These results are consistent with competition of
302 DNA and membranes over the same binding sites, located at the interior of the tube, as
303 recently suggested for human CHMP1B (31). Alternatively, the presence of DNA may
304 change the biophysical properties of the tube, thereby resisting the deformation of the
305 tube needed to facilitate membrane remodeling from within. Future experiments
306 allowing direct visualization of ESCRT-III proteins, DNA and the membrane at high
307 resolution are needed in order to examine these models and to resolve the intimate
308 relationship between these three partners.

309

310 Overall, the Loki ESCRT-III filaments characterized here, share more similar
311 characteristics to human CHMP1B-IST1 filaments than to human CHMP2A-CHMP3 or
312 yeast snf7 (human CHMP4B) filaments. Filaments of both Asgard ESCRT-III and
313 human CHMP1B, were shown to assemble into homo- and co- polymers with the latter
314 being more constricted; both filaments were reported to bind DNA in vitro; and both
315 deformed membranes via binding to the inner side of the filamentous tube. Consistently,
316 we recently showed that both Loki CHMP4-7 and human CHMP1B associate with
317 chromatin when expressed in mammalian cells (26). We therefore suggest that Asgard
318 ESCRT-IIIs are functionally most similar to CHMP1B in the eukaryotic ESCRT-III
319 system.

320

321 The biological function of Asgard ESCRTs has yet to be defined. The findings that Loki
322 ESCRT-III filaments can bind both DNA and membranes raises a few attractive
323 possibilities. First, given the established role of ESCRTs in cell division in TACK
324 archaea and in eukaryotes, it is possible that the ESCRT machinery manifest a basic
325 cell division machinery capable of orchestrating DNA segregation and membrane
326 splitting (22-25). In this regard, the ability of DNA to retain extensive membrane
327 deformation may represent a biological mechanism to avoid premature membrane
328 constriction during cell division. Second, the ESCRT complex may have been involved
329 in nuclear membrane formation during eukaryogenesis, by bringing together
330 membranes and DNA and facilitating DNA encapsulation by membranes. In this
331 respect, mammalian ESCRT-III proteins have been shown to mediate sealing of the
332 nuclear membrane post cell division and to regulate the attachment of heterochromatin
333 to the newly formed nuclear envelop (33-35). Moreover, we recently reported that Loki
334 CHMP 4-7 is targeted to the nucleus when over expressed in eukaryotic cells (26).
335 Finally, the membrane binding experiments performed here were done using
336 eukaryotic-like phospholipids, which are fundamentally different from archaeal lipids but
337 may resemble the lipid composition of the newly formed nuclear membrane. Therefore,
338 the ESCRT-III system encoded by Asgard archaea could have contributed to the

339 membrane remodeling that occurred during the formation of the phospholipids-based
340 nuclear membrane.
341
342 MATERIALS AND METHODS
343 **Cloning**
344 Open reading frames (ORFs) from Loki MAG sp. GC14_75, encoding for CHMP1-3 and
345 CHMP4-7 genes were obtained from NCBI (accession numbers KKK42122.1,
346 KKK44605.1, respectively) were amplified by PCR and sub-cloned into pSH21 vector
347 subsequently to the TEV cleavage tag that followed an N terminal polyhistidine and
348 MBP protein tags (a kind gift from Eyal Gur, BGU, Israel)(36). Plasmids were verified by
349 sequencing.
350
351 **Protein Expression and Purification**
352 pSH21 plasmids containing Loki CHMP1-3 or CHMP4-7 were expressed Escherichia
353 coli BL21 strain and incubated in LB 50 µg/mL Ampicillin at 37°C until reaching O.D. of
354 0.6. Then, induction with 0.5 mM IPTG was performed and the cultures were grown at
355 30°C for 3-4 hours. Cells were then resuspended and lysed by sonication in buffer A (25
356 mM Hepes pH= 8, 500 mM NaCl, 10% glycerol, 15 mM 2-mercaptoethanol, 10 mM
357 imidazole) supplemented with protease inhibitor cocktail (cOmplete ultra-tablets, EDTA-
358 free, Roche) and 500 µg/ml DNase I (10104159001; Roche Diagnosis GmbH, Manheim,
359 Germany), and the supernatant was clarified by centrifugation (25,000 g, 40 mins, 4°C).
360 For CHMP4-7 purification, supernatant was subjected to HisPur™ Ni-NTA Resin
361 (88222; Thermo Fisher Scientific, Weltham, MA) column and eluted in buffer B (buffer A
362 supplemented with 50 mM imidazole). Protein tags were then removed using a TEV
363 protease (1 mg/10 mg protein) in buffer C (50mM Tris-HCL pH=7.4, 10% glycerol, 500
364 mM NaCl, 15 mM 2-mercaptoethanol). Finally, a second Ni-NTA step was performed
365 using buffer C and the flow-through was collected.
366 For CHMP1-3 purification, supernatant was subjected to Ni-NTA column and eluted in
367 buffer B. Samples were then subjected to amylose resin (E8021; NEB, Frankfurt,
368 Germany) in buffer D (20mM Tris pH=7.4, 500 mM NaCl, 10mM β-Mercaptoethanol,
369 10% Glycerol) and eluted in buffer D supplemented with 10mM maltose. Protein tags

370 were then removed using a TEV protease (1 mg/10 mg protein) in buffer C (50mM Tris-
371 HCL pH=7.4, 10% glycerol, 500 mM NaCl, 15 mM 2-mercaptoethanol). Finally, a
372 second Ni-NTA step was performed using buffer C and the flow-through was collected.
373 Purified proteins were verified my mass spectrometry.
374
375 For polymerization, proteins were incubated in buffer E (25mM Tris pH=7.6, 50 mM KCl)
376 for 5 hours at RT at the indicated conditions. For DNA experiments,
377 ATCCACCTGTACATCAACTCGCCCGGCGGCTCGATCAGCG (40 bases probe), ss or
378 ds were used at the indicted concentrations. DNase I (10104159001; Roche Diagnosis
379 GmbH, Manheim, Germany) was added at 20mg/ml concentrations when indicated.
380
381 **Preparation of small unilamellar vesicles (SUVs)**
382 Chloroform Lipid solutions (DOPC or DOPS) were purchased from Avanti Polar Lipids
383 Inc. (Albaster, AL, USA catalog number 850375, 840035). Lipid mixtures of
384 DOPC/DOPS 1:1 molar ratio and pure DOPC were prepared at a total concentration of
385 1 mg/ml in Tris 20 mM, KCl 50 mM, pH 7.8 were prepared. Each lipid suspension was
386 extruded 20 times via a 100 nm polycarbonate membrane using a mini-extruder (Avanti
387 Polar Lipids, Alabaster, AL, USA). In the final stage, the vesicles were mixed with the
388 Asgard Loki ESCRT-III filaments. All experiments were done with 8 μM ESCRT-III and
389 124 μM vesicles in a buffer of Tris 25 mM, KCl 50 mM, at pH 7.6.
390
391 **Negative Stain grid preparation and imaging**
392 The negative stain samples for TEM analysis were prepared in the following way: 300
393 mesh copper grids (Ted Pella, Prod No. 01813-F) were glow discharged to enhance
394 hydrophilicity of their surface. Next, 2.5 uL of the sample was applied on to the grid and
395 the excess liquid was blotted with filter paper after 1 minute. The grid was dried in air for
396 1 minute, following by applying 5 uL of uranyl acetate 2% solution (SPI CAS# 6159-44-
397 0) for negative staining to increase the sample contrast. Next, the grid was blotted ones
398 more to remove the excess uranyl acetate. Finally, the grid was dried in air before
399 insertion into the microscope. The imaging of the samples was performed with Thermo

400 Fisher Scientific Talos F200C transmission electron microscope operating at 200 kV.
401 The images were taken with Ceta 16M CMOS camera.
402
403 **Cryo-electron microscopy**
404 Sample preparation: 3 μL of proteins / proteins-phospholipids mix samples were gently
405 deposited on glow discharged Quantifoil R 1.2/1.3 holey carbon grids (Quantifoil Micro
406 Tools GmbH, Germany). Samples were manually blotted for four seconds at room
407 temperature and vitrified by rapidly plunging into liquid ethane using a home-built
408 plunging apparatus. The frozen samples were stored in liquid nitrogen until imaging.
409 **Micrographs acquisition:** Samples were loaded under cryogenic conditions and
410 imaged in low dose mode on a FEI Tecnai F30 Polara microscope (FEI, Eindhoven)
411 operated at 300 kV. Micrographs were collected using SerialEM, at a calibrated pixel
412 size of 1.1 Å by a K2 Summit direct electron detector fitted behind an energy filter
413 (Gatan Quantum GIF) set to ±10 eV around zero-loss peak with total electron dose of
414 80 ē/Å^2. Each dose-fractionated movie had 50 frames, micrographs sums were aligned
415 in SerialEM.
416
417 **Cryo-tomography.** Micrographs were acquired with a FEI Tecnai F30 Polara
418 microscope (FEI, Eindhoven) operated at 300 kV, using a K2 Summit direct electron
419 detector fitted behind an energy filter (Gatan Quantum GIF), set to ±10 eV slit around
420 the zero-loss peak. Pixel size at the sample plane was 2.3 Å. The camera was operated
421 in counting mode at a dose rate of 6−7 ē/pixels/sec. Tilt series of 41 exposures from
422 −21° to +60° and back to -60° in 3° intervals and a total dose of ~ 120 ē /Å^2 were
423 collected with Serial-EM. Tilt series were aligned, and tomograms were reconstructed
424 using eTomo (IMOD4.11 package) (37). Movies were generated in imageJ.
425
426 **Measurements and statistical analysis**
427 Filament length and diameter measurements were performed in Velox software version
428 3.5 (Thermo Fisher Scientific, Inc.).
429 Statistical analysis was performed in Graph Pad Prism version 9.00 (La Jolla, CA,
430 USA). Unless specified otherwise, comparison between two groups was calculated by

one way ANOVA * p- value ≤ 0.1, **p- value ≤ 0.01, ***p- value ≤ 0.001, ****p-value ≤ 0.0001.

ACKNOWLEDMENTS

We thank the laboratories of Eyal Gur (BGU) and Eyal Arbely (BGU) for their practical advice on proteins expression and purifications and for kindly sharing their reagents and equipment with us. We also thank Itzik Mizrahi (BGU) and Ori Avinoam (WIS) for constructive feedback on the project. Last, we thank all members of the Elia lab for critical feedback throughout the project. The Elia laboratory is funded by the Israeli Science Foundation (ISF) Grant no. 1323/18. ABG is grateful to the Israel Science Foundation for financial support (grant 2101/20).

AUTHOR CONTRIBUTIONS

NE and DN conceptualized the project. NM performed and analyzed all experiments. GH and AB, were in charge of experiments using SUVs. AU acquired negative stain TEM images. RZ acquired and analyzed cryo-EM data. NE, DN, AB and RZ were involved in experimental design and data analysis. NE wrote the manuscript. All authors read and revised the manuscript.

Competing Interest Statement: We declare no competing interest

REFERENCES

461 1. K. Zaremba-Niedzwiedzka *et al.*, Asgard archaea illuminate the origin of eukaryotic
462 cellular complexity. *Nature* **541**, 353-358 (2017).
463 2. F. MacLeod, G. S. Kindler, H. L. Wong, R. Chen, B. P. Burns, Asgard archaea: Diversity,
464 function, and evolutionary implications in a range of microbiomes. *AIMS Microbiol* **5**, 48-
465 61 (2019).
466 3. A. Spang *et al.*, Complex archaea that bridge the gap between prokaryotes and
467 eukaryotes. *Nature* **521**, 173-179 (2015).
468 4. E. Neveu, D. Khalifeh, N. Salamin, D. Fasshauer, Prototypic SNARE Proteins Are Encoded
469 in the Genomes of Heimdallarchaeota, Potentially Bridging the Gap between the
470 Prokaryotes and Eukaryotes. *Curr Biol* **30**, 2468-2480 e2465 (2020).
471 5. Z. Lu *et al.*, Coevolution of Eukaryote-like Vps4 and ESCRT-III Subunits in the Asgard
472 Archaea. *mBio* **11** (2020).
473 6. T. Hatano *et al.*, Asgard archaea shed light on the evolutionary origins of the eukaryotic
474 ubiquitin-ESCRT machinery. *Nat Commun* **13**, 3398 (2022).
475 7. Y. Caspi, C. Dekker, Dividing the Archaeal Way: The Ancient Cdv Cell-Division Machinery.
476 *Front Microbiol* **9**, 174 (2018).
477 8. J. H. Hurley, ESCRTs are everywhere. *EMBO J* **34**, 2398-2407 (2015).
478 9. Y. A. M. Alonso, S. M. Migliano, D. Teis, ESCRT-III and Vps4: a dynamic multipurpose tool
479 for membrane budding and scission. *FEBS J* **283**, 3288-3302 (2016).
480 10. J. McCullough, L. A. Colf, W. I. Sundquist, Membrane fission reactions of the mammalian
481 ESCRT pathway. *Annu Rev Biochem* **82**, 663-692 (2013).
482 11. C. Caillat, S. Maity, N. Miguet, W. H. Roos, W. Weissenhorn, The role of VPS4 in ESCRT-III
483 polymer remodeling. *Biochem Soc Trans* **47**, 441-448 (2019).
484 12. S. Maity *et al.*, VPS4 triggers constriction and cleavage of ESCRT-III helical filaments. *Sci*
485 *Adv* **5**, eaau7198 (2019).
486 13. B. E. Mierzwa *et al.*, Dynamic subunit turnover in ESCRT-III assemblies is regulated by
487 Vps4 to mediate membrane remodelling during cytokinesis. *Nat Cell Biol* **19**, 787-798
488 (2017).
489 14. A. K. Pfitzner *et al.*, An ESCRT-III Polymerization Sequence Drives Membrane
490 Deformation and Fission. *Cell* **182**, 1140-1155 e1118 (2020).
491 15. W. M. Henne, N. J. Buchkovich, Y. Zhao, S. D. Emr, The endosomal sorting complex
492 ESCRT-II mediates the assembly and architecture of ESCRT-III helices. *Cell* **151**, 356-371
493 (2012).
494 16. I. Goliand *et al.*, Resolving ESCRT-III Spirals at the Intercellular Bridge of Dividing Cells
495 Using 3D STORM. *Cell Rep* **24**, 1756-1764 (2018).
496 17. J. Guizetti *et al.*, Cortical constriction during abscission involves helices of ESCRT-III-
497 dependent filaments. *Science* **331**, 1616-1620 (2011).
498 18. J. McCullough *et al.*, Structure and membrane remodeling activity of ESCRT-III helical
499 polymers. *Science* **350**, 1548-1551 (2015).
500 19. S. Lata *et al.*, Helical structures of ESCRT-III are disassembled by VPS4. *Science* **321**,
501 1354-1357 (2008).
502 20. B. P. Frohn, T. Hartel, J. Cox, P. Schwille, Tracing back variations in archaeal ESCRT-based
503 cell division to protein domain architectures. *PLoS One* **17**, e0266395 (2022).

504 21. J. Liu *et al.*, Bacterial Vipp1 and PspA are members of the ancient ESCRT-III membrane-
505 remodeling superfamily. *Cell* **184**, 3660-3673 e3618 (2021).
506 22. A. C. Lindas, E. A. Karlsson, M. T. Lindgren, T. J. Ettema, R. Bernander, A unique cell
507 division machinery in the Archaea. *Proc Natl Acad Sci U S A* **105**, 18942-18946 (2008).
508 23. R. Y. Samson, T. Obita, S. M. Freund, R. L. Williams, S. D. Bell, A role for the ESCRT
509 system in cell division in archaea. *Science* **322**, 1710-1713 (2008).
510 24. R. Y. Samson *et al.*, Molecular and structural basis of ESCRT-III recruitment to
511 membranes during archaeal cell division. *Mol Cell* **41**, 186-196 (2011).
512 25. G. Tarrason Risa *et al.*, The proteasome controls ESCRT-III-mediated cell division in an
513 archaeon. *Science* **369** (2020).
514 26. D. Nachmias *et al.* (2022) Asgard ESCRT-III and VPS4 reveal evolutionary conserved
515 chromatin binding properties of the ESCRT machinery. in *bioRxiv*
516 27. K. Azad *et al.* (2022) Structural basis of CHMP2A-CHMP3 ESCRT-III polymer assembly and
517 membrane cleavage. in *bioRxiv*.
518 28. Y. Olmos, The ESCRT Machinery: Remodeling, Repairing, and Sealing Membranes.
519 *Membranes (Basel)* **12** (2022).
520 29. B. Junglas *et al.*, PspA adopts an ESCRT-III-like fold and remodels bacterial membranes.
521 *Cell* **184**, 3674-3688 e3618 (2021).
522 30. H. C. Nguyen *et al.*, Membrane constriction and thinning by sequential ESCRT-III
523 polymerization. *Nat Struct Mol Biol* **27**, 392-399 (2020).
524 31. N. Talledge *et al.* (2018) The ESCRT-III proteins IST1 and CHMP1B assemble
525 around nucleic acids. in *bioRxiv*.
526 32. T. K. Gupta *et al.*, Structural basis for VIPP1 oligomerization and maintenance of
527 thylakoid membrane integrity. *Cell* **184**, 3643-3659 e3623 (2021).
528 33. G. H. Pieper, S. Sprenger, D. Teis, S. Oliferenko, ESCRT-III/Vps4 Controls
529 Heterochromatin-Nuclear Envelope Attachments. *Dev Cell* **53**, 27-41 e26 (2020).
530 34. Y. Olmos, L. Hodgson, J. Mantell, P. Verkade, J. G. Carlton, ESCRT-III controls nuclear
531 envelope reformation. *Nature* **522**, 236-239 (2015).
532 35. M. Vietri *et al.*, Spastin and ESCRT-III coordinate mitotic spindle disassembly and nuclear
533 envelope sealing. *Nature* **522**, 231-235 (2015).
534 36. Y. Elharar *et al.*, Survival of mycobacteria depends on proteasome-mediated amino acid
535 recycling under nutrient limitation. *EMBO J* **33**, 1802-1814 (2014).
536 37. D. N. Mastronarde, Automated electron microscope tomography using robust prediction
537 of specimen movements. *J Struct Biol* **152**, 36-51 (2005).
538
539
540
541
542
543
544

545 FIGURES AND FIGURES LEGENDS

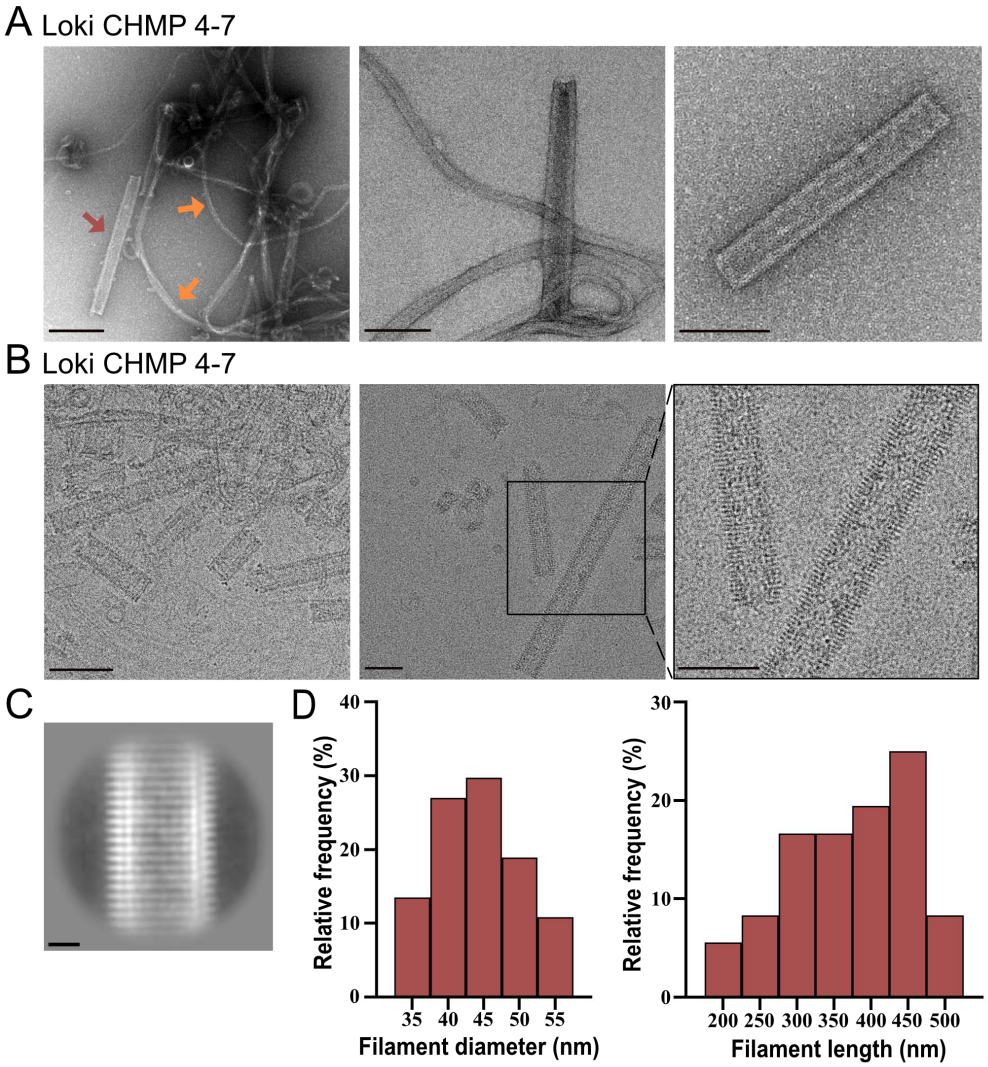

546

547 **Fig 1. Loki CHMP4-7 protein self-assemble into filaments and helical tubes.**
548 **A.** Negative- stain TEM micrographs of Loki CHMP4-7 homo-filaments. Representative
549 zoomed-out (left, scale = 200 nm) and zoomed- in (middle and right, scale = 100 nm)
550 images are shown. Orange arrows indicate filaments, red arrow indicates a helical tube.
551 **B.** Representative Cryo-EM micrographs of Loki CHMP4-7 homo-polymers. Left,
552 zoomed-out image (Scale = 100 nm), middle and right, zoomed-in images (Scale = 50
553 nm). Box in middle panel specify the zoomed-in region shown to the right. **C.** A
554 representative 2D class average of 502 particles extracted from CHMP 4-7 projections.
555 Scale = 100 Å. **D.** Measurements of Loki CHMP4-7 helical diameters (left, n = 37) and

length (right, n = 36) obtained from negative stain TEM images acquired from two independent experiments. Averaged CHMP 4-7 helical tube diameter 44nm±30.9.

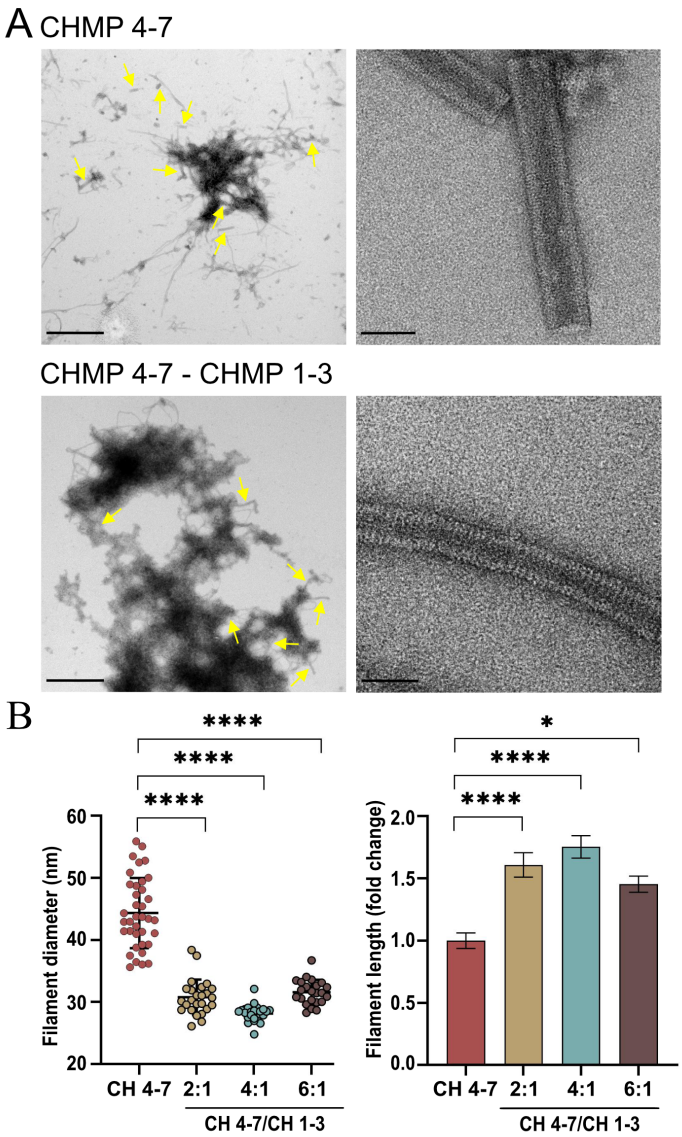

586

587 **Fig 2. Loki CHMP4-7 and CHMP1-3 co-polymers assemble into helical tubes**
588 **exhibiting different properties from CHMP 4-7 homo-polymers.**
589 **A.** Representative Negative- stain TEM images of Loki CHMP4-7 homo-polymers
590 (upper panels) and CHMP4-7-CHMP1-3 co-polymers (bottom panels, 2:1 molar ratio).
591 Zoomed- out (left, scale = 1 μm) and zoomed- in (right, scale = 50 nm) images are
592 shown. Yellow asterisks indicate helical tubes. **B**. Measurements of CHMP4-7-CHMP1-
593 3 hetero-filaments diameters (left) and length (right) at the indicated molar ratios
594 obtained from negative stain TEM images. Averaged diameters (nm): 2:1 ratio, 31±7.7;
595 4:1 ratio 28±1.6, 6:1 ratio 32±3.8. n = 25 for each condition.

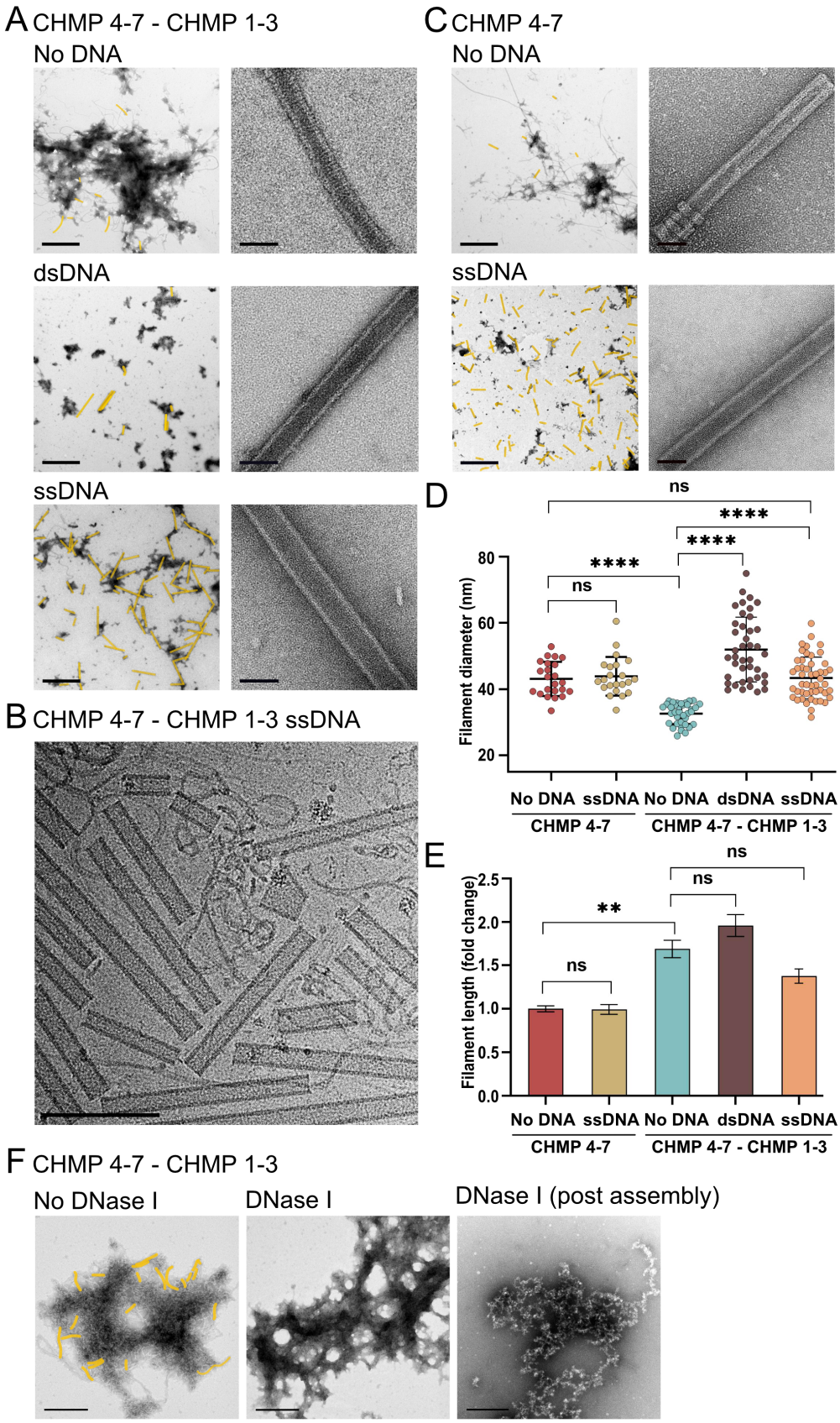
A CHMP 4-7 - CHMP 1-3
No DNA
dsDNA
ssDNA
B CHMP 4-7 - CHMP 1-3 ssDNA
C CHMP 4-7
No DNA
ssDNA
D
ns
****
****
****
ns
Filament diameter (nm)
80
60
40
20
No DNA ssDNA No DNA dsDNA ssDNA
CHMP 4-7
CHMP 4-7 - CHMP 1-3
E
ns
ns
**
ns
Filament length (fold change)
2.5
2.0
1.5
1.0
0.5
0.0
No DNA ssDNA No DNA dsDNA ssDNA
CHMP 4-7
CHMP 4-7 - CHMP 1-3
F CHMP 4-7 - CHMP 1-3
No DNase I
DNase I
DNase I (post assembly)

596

597 **Fig 3. Organization into helical tubes is increased in the presence of DNA**
598 **A.** Negative- stain TEM micrographs of CHMP 4-7-CHMP 1-3 co- polymers (2:1 molar
599 ratio) in the presence of 4.6 μM 40 bases oligonucleotides (ssDNA or dsDNA, as
600 indicated). Representative zoomed- out (left, Scale = 1 μm) and zoomed- in (right, Scale
601 = 50 nm) images are shown. Helical tubes are colored in yellow in zoomed out images
602 to highlight the observed increase in tubes (raw images are provided in Sup Fig 2A). **B**.
603 Representative Cryo-EM images of CHMP 4-7– CHMP 1-3 co-polymers (molar ratio,
604 4:1) in the presence of ssDNA. Scale = 200 nm. **C.** Negative- stain TEM micrographs of
605 CHMP 4-7 homo-polymers in the presence of 4.6 μM 40 bases ssDNA. Representative
606 zoomed- out (left, Scale = 1 μm) and zoomed- in (right, Scale = 50 nm) images are
607 shown. Helical tubes are colored in yellow in zoomed out images to highlight the
608 observed increase in tubes (raw images are provided in Sup Fig 2B). **D-E** Diameter (**D**)
609 and length (**E**) measurements of helical tubes formed by homo- and the co-polymers
610 (2:1 ratio) in the presence of nucleic acids obtained from negative stain TEM images.
611 Averaged diameters (nm): CHMP4-7 ssDNA 43.9±33, n=21; CHMP4-7-CHMP1-3 2:1
612 dsDNA 51.9±94, n=44; CHMP4-7-CHMP1-3 2:1 ssDNA 43.9±58, n=48). **F**.
613 Representative Negative- stain TEM images of co-polymers (molar ratio 2:1) upon
614 addition of 20 mg/ml DNase I during (middle panel) or after (right panel) polymerization.
615 Helical tubes are colored in yellow. Scale =200 nm. Data was reproduced in four
616 independent experiments.
617
618
619
620
621
622
623
624
625
626
627

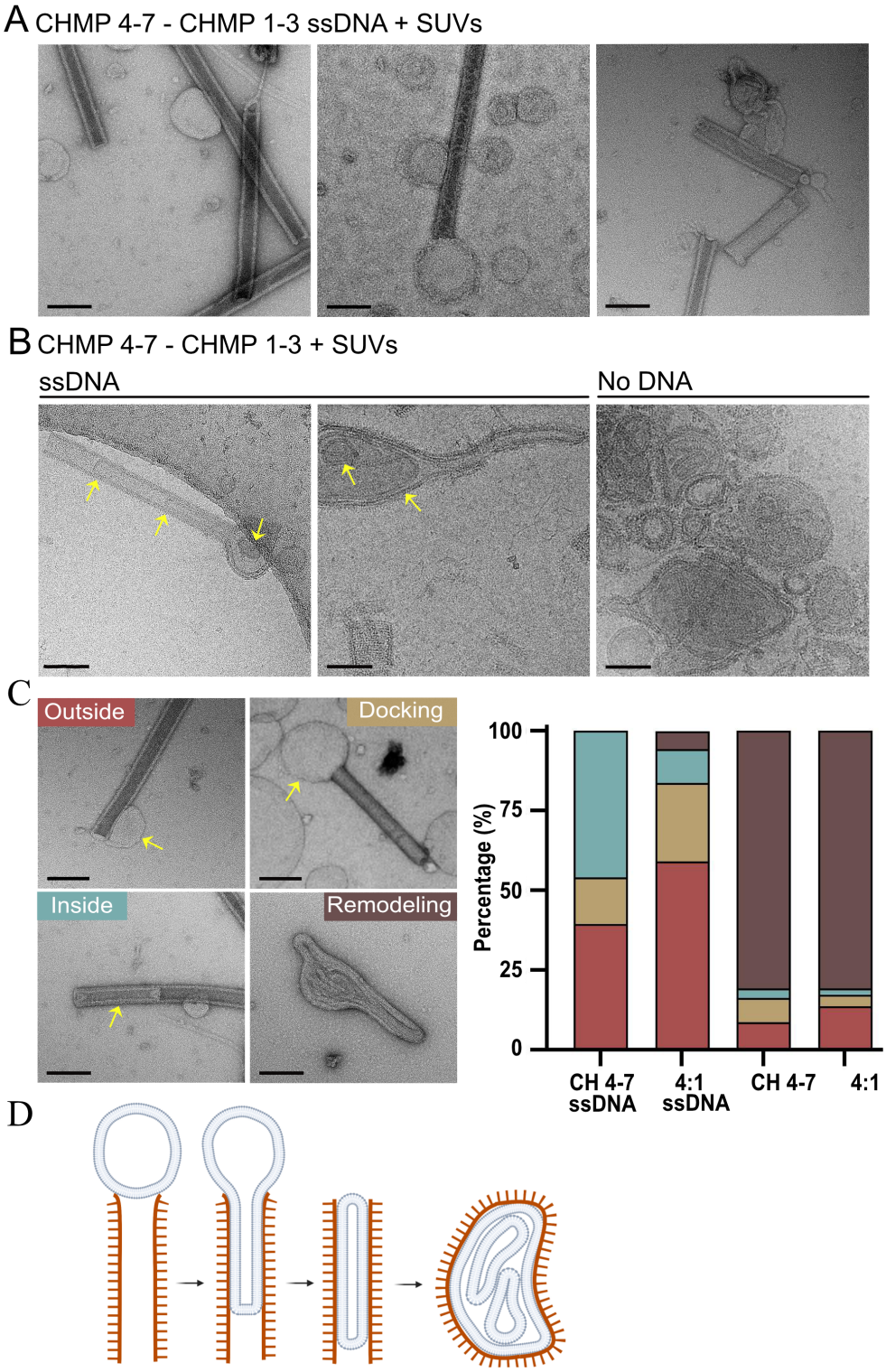
A CHMP 4-7 - CHMP 1-3 ssDNA + SUVs
B CHMP 4-7 - CHMP 1-3 + SUVs
ssDNA
No DNA
C
Outside
Docking
Inside
Remodeling
Percentage (%)
100
75
50
25
0
CH 4-7 ssDNA
4:1 ssDNA
CH 4-7
4:1
D

628

629 **Fig 4. Loki ESCRT-III filaments induce membrane remodeling**

630 **A-B.** Representative Negative- stain TEM (**A**) and Cryo-EM images (**B**) of CHMP4-7-
631 CHMP1-3 (molar ratio, 4:1) polymerized in the presence of ssDNA (10 μM) and
632 incubated with SUVs (DOPC:DOPS, 1:1 ratio). Scale = 100 nm. Arrows in **B** specify
633 internalized vesicles. Reconstructed tomograms of filaments collected from the same
634 grid are provided in Sup. movies 1 and 2. **C**. Percentages of the different types of
635 vesicle-tube interactions observed under the specified conditions. Left panel,
636 represented negative-stain images of the four types of interactions quantified. Outside,
637 attachment of SUV to the outside of the helical tube (type 1); Docking, binding of the
638 vesicle to the tip of the helical tube (type 2); Inside, invagination of the SUV to the
639 helical tube (type 3); Remodeling, deformation of both the vesicles and the ESCRT-III
640 helical tube (type 4). Data was quantified from negative stain imaged obtained in 3
641 independent experiments (n = CHMP4-7 ssDNA, 124; CHMP4-7-CHMP1-3 ssDNA,
642 159; CHMP4-7, 197; CHMP4-7-CHMP1-3, 161). Scale = 100 nm. Chi square statistical
643 analysis show a significant difference in the distributions of CHMP4-7 ssDNA vs
644 CHMP4-7 (****p- value ≤ 0.0001), CHMP4-7-CHMP1-3 ssDNA vs CHMP4-7-CHMP1-3
645 (****p- value ≤ 0.0001), and CHMP4-7 ssDNA vs CHMP4-7-CHMP1-3 ssDNA (****p-
646 value ≤ 0.0001). No significance was found in the distributions of CHMP4-7 vs CHMP4-
647 7-CHMP1-3. **D**. A suggested model for Loki ESCRT-III mediated vesicle remodeling.
648 Vesicles dock at the tip of the ESCRT-III tube. Docking allows the vesicle to directly
649 interact with the interior of the tube, leading to deformation and invagination of the
650 vesicle by the ESCRT-III filament. This process occurs repeatedly leading to the
651 formation of a complex membrane network inside the helical tube, which pushes the
652 ESCRT-III tube from the inside and ultimately causing deformation and remodeling of
653 the tube. This stage is inhibited in the presence of DNA, resulting the accumulation of
654 ESCRT-III-SUV interactions in all the stages that preceded this complete remodeling
655 stage.
656
657
658
659